

## Lattice dynamics of FeSb<sub>2</sub>

N. Lazarević,<sup>1</sup> M. M. Radonjić,<sup>2</sup> D. Tanasković,<sup>2</sup> Rongwei Hu\*,<sup>3</sup> C. Petrovic,<sup>3</sup> and Z. V. Popović<sup>1</sup>

<sup>1</sup>*Center for Solid State Physics and New Materials, Institute of Physics Belgrade,*

*University of Belgrade, Pregrevica 118, 11080 Belgrade, Serbia*

<sup>2</sup>*Scientific Computing Laboratory, Institute of Physics Belgrade,*

*University of Belgrade, Pregrevica 118, 11080 Belgrade, Serbia*

<sup>3</sup>*Condensed Matter Physics and Materials Science Department,*

*Brookhaven National Laboratory, Upton, New York 11973-5000, USA*

The lattice dynamics of FeSb<sub>2</sub> is investigated by the first-principles DFT calculations and Raman spectroscopy. All Raman and infrared active phonon modes are properly assigned. The calculated and measured phonon energies are in good agreement. We have observed strong mixing of the A<sub>g</sub> symmetry modes, with the intensity exchange in the temperature range between 210 K and 260 K. The A<sub>g</sub> modes repulsion increases by doping FeSb<sub>2</sub> with Co, with no signatures of the electron-phonon interaction for these modes.

PACS numbers: 63.20.D-; 71.15.Mb; 71.28.+d; 78.30.Hv;

### I. INTRODUCTION

FeSb<sub>2</sub> is a strongly correlated narrow-gap semiconductor which has recently attracted a lot of attention due to its unusual thermoelectric properties.[1–6] It was shown that FeSb<sub>2</sub> has colossal thermopower  $S$  at 10 K (range from 1 mV/K to 45 mV/K[5, 7]) and the largest power factor  $S^2\sigma$  ever reported.[5, 7–9] The phonon contribution to  $S$  remains controversial.[10] Also, the thermal conductivity  $\kappa$  of FeSb<sub>2</sub> is relatively high and around 10 K is dominated by the phonons.[5] Consequently, full knowledge of FeSb<sub>2</sub> lattice dynamics is necessary in order to understand the low temperature transport and thermodynamic properties of this material.

The infrared active phonon frequencies of FeSb<sub>2</sub> were obtained from the polarized far-infrared reflectivity spectra.[11] From E||b polarized reflectivity measurements on (102) plane of FeSb<sub>2</sub> single crystal, Perucchi *et al.* observed four modes at 106.4, 231, 257 and 271 cm<sup>-1</sup> at 10 K (factor group analysis predicts 3B<sub>2u</sub> modes for this polarization configuration). For E⊥b polarization, both B<sub>1u</sub> and B<sub>3u</sub> symmetry modes can be observed from (102) plane. Three (of four) modes at 121, 216 and 261.4 cm<sup>-1</sup> are observed for this polarization. Raman scattering measurements on FeSb<sub>2</sub> were published in Refs. 12–15. Lutz and Müller[12] observed two Raman active modes at about 175 and 154 cm<sup>-1</sup> on hot-pressed samples, and assigned them as the A<sub>g</sub> symmetry

modes. In contrast, Racu *et al.*[13] observed three Raman modes at about 150, 157 and 180  $\text{cm}^{-1}$  using polarized Raman scattering measurements on  $\text{FeSb}_2$  single crystals and assigned them as the  $B_{1g}$ ,  $A_g$  and  $B_{1g}$  symmetry modes, respectively. Finally, all six Raman active modes of  $\text{FeSb}_2$  predicted by the factor group analysis ( $2A_g+2B_{1g}+B_{2g}+B_{3g}$ ) were observed in Ref. 14. Polarized Raman scattering spectra of the  $\text{Fe}_{1-x}\text{M}_x\text{Sb}_2$  ( $\text{M}=\text{Cr},\text{Co}$ ) single crystals was studied in Ref. 15. The linewidths and energies of the Raman modes were analyzed as a function of doping  $x$  and temperature. Strong electron-phonon interaction, observed for the  $B_{1g}$  symmetry mode of pure  $\text{FeSb}_2$ , produces significant mode asymmetry. The electron-phonon interaction is drastically reduced with increasing concentration of Co and Cr in  $\text{Fe}_{1-x}(\text{Co},\text{Cr})_x\text{Sb}_2$ . The mixing of the  $A_g$  symmetry phonon modes has been observed both in pure and Cr-doped samples.[15]

In this paper we report *ab initio* study of the lattice dynamics of  $\text{FeSb}_2$ . The calculated phonon energies in the  $\Gamma$  point are in good agreement with experimental data. Phonon density of state show a gap at about 175  $\text{cm}^{-1}$ , which divides a low frequency region where vibration modes are mostly Raman active from a high frequency region where only infrared active modes appear. The calculated phonon dispersions for two  $A_g$  symmetry modes indicates strong mode mixing. This is indeed observed in our polarized Raman scattering spectra. The  $A_g$  mode intensity exchange in the temperature range between 210 K and 260 K agrees well with theoretical calculations, excluding any additional temperature dependent electron phonon coupling for these modes. The mode repulsion increases with Co doping.

## II. EXPERIMENT

Single crystals of  $\text{FeSb}_2$  and  $\text{Fe}_{0.75}\text{Co}_{0.25}\text{Sb}_2$  were grown by the self-flux method and characterized as described elsewhere.[1] The Raman scattering measurements were performed using Jobin Yvon T64000 Raman system in micro-Raman configuration. The 514.5 nm line of an  $\text{Ar}^+/\text{Kr}^+$  mixed gas laser was used as an excitation source. Focusing of the laser beam was realized with a long distance microscope objective (magnification 50 $\times$ ). We have found that laser power level of 0.02 mW on the sample is sufficient to obtain Raman signal and, except signal to noise ratio, no changes of the spectra were observed as a consequence of laser heating by further lowering laser power. The corresponding excitation power density was less than 0.1  $\text{kW}/\text{cm}^2$ . Low temperature measurements were performed between 15 K and 300 K using KONTI CryoVac continuous Helium flow cryostat with 0.5 mm thick window. Raman scattering measurements of pure and Co doped  $\text{FeSb}_2$  samples were performed using the  $(10\bar{1})$  oriented  $\text{FeSb}_2$  samples. Selection rules for parallel

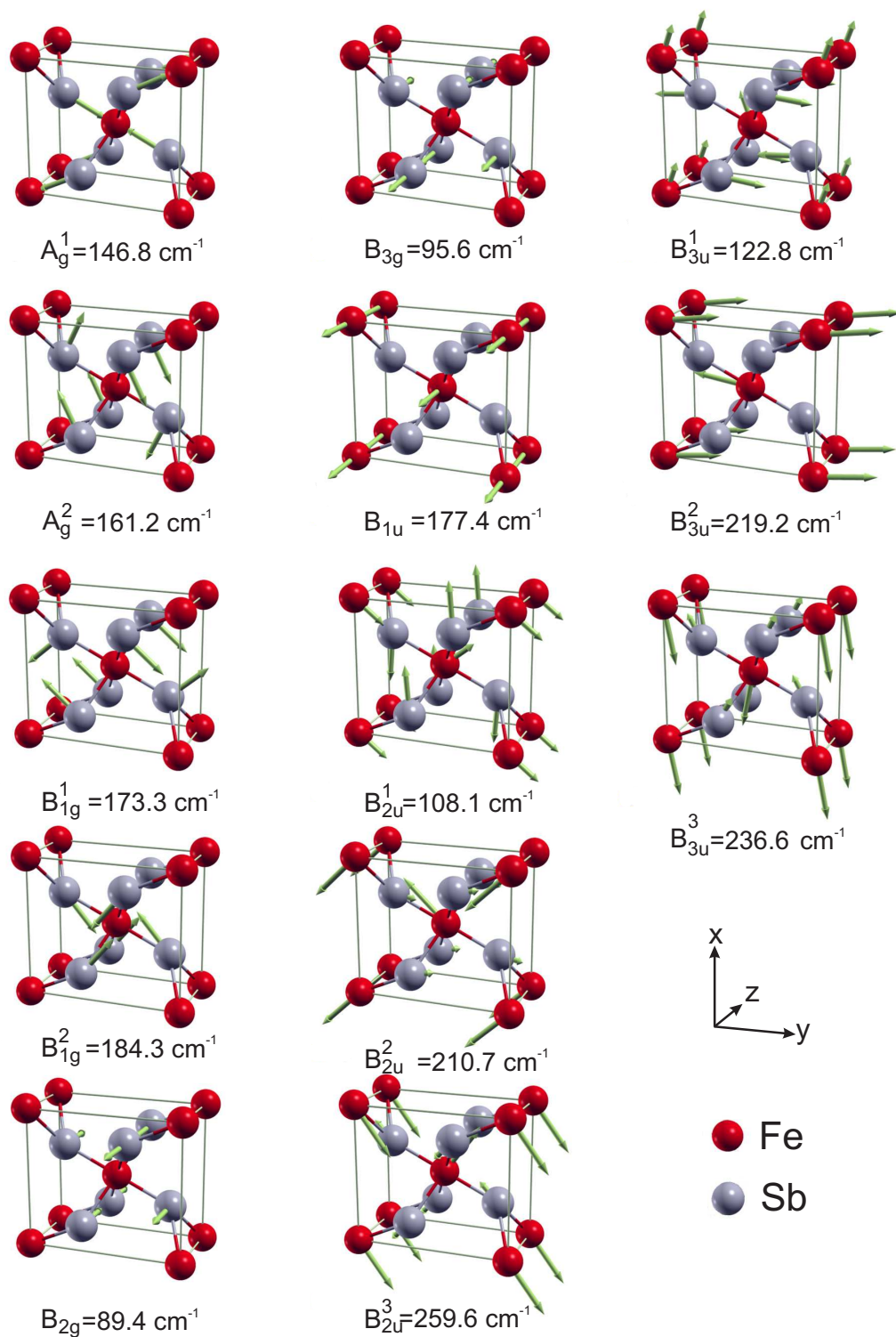


FIG. 1. (Color online) Atomic displacement patterns for the vibrational modes of  $\text{FeSb}_2$ . The length of the arrows are proportional to square root of the vibration amplitudes.

and crossed polarization from the  $(10\bar{1})$  plane of the orthorhombic crystal symmetry and the mode assignment have been presented in Ref. 14.

### III. NUMERICAL METHOD

FeSb<sub>2</sub> crystallizes in the orthorhombic marcasite-type structure of the centrosymmetric Pnmm ( $D_{2h}^{12}$ ) space group, with two formula units ( $Z=2$ ) per unit cell.[16, 17] Basic structural unit is built up of Fe atoms surrounded by deformed Sb octahedra. These structural units are corner sharing in the (ab) plane and edge sharing along the  $c$ -axis. Two Fe atoms are in (2a) Wyckoff positions at (0,0,0) and four Sb atoms are in (4g) Wyckoff positions at  $(0,u,v)$  of the Pnmm space group. Our density functional theory (DFT) calculations are performed within generalized gradient approximation (GGA) with PW91 exchange-correlation functional which is used to calculate ultra-soft pseudopotentials,[18] as implemented in the QUANTUM ESPRESSO package.[19] Iron (antimony) pseudopotential takes into account  $3s^2 3p^6 4s^2 3d^6 (4d^{10} 5s^2 5p^3)$  electron states for the valence electrons. The Brillouin zone was sampled with an  $8 \times 8 \times 8$  Monkhorst-Pack  $\mathbf{k}$ -space mesh and with the Marzari-Vanderbilt cold smearing (0.005Ry).[20] The obtained optimized structural parameters are  $a=5.859 \text{ \AA}$ ,  $b=6.583 \text{ \AA}$ ,  $c=3.812 \text{ \AA}$ ,  $u=0.1882$ , and  $v=0.3554$ , which are in good agreement with the experiment. Our band structure calculations agree well with the previously reported. [10, 21, 22]

### IV. RESULTS AND DISCUSSION

The lattice dynamics is investigated by the density functional perturbation theory (DFPT)[23] within the theory of linear response. This method includes calculations of charge response to the lattice distortions (allowed by the symmetry operations) for the specified vectors in the first Brillouin zone. Calculations start from the previously calculated ground state atomic and electronic configuration and continue with the self-consistent calculations of the charge response for each different displacement. The normal modes of the optical active phonons (in the  $\Gamma$  point) are given in Fig. 1. Because Fe ions are located in the center of inversion of Pnmm space group, they do not contribute to the Raman scattering process, i.e. the Raman modes of FeSb<sub>2</sub> originate only from the Sb atoms vibrations, in a manner illustrated in Fig. 1. In the case of infrared active modes, both the Fe and Sb atoms contribute to the normal modes, see Fig.1.

In order to obtain the phonon dispersion curves, we have calculated the phonon frequencies at

TABLE I. Raman and infra-red active mode energies (in  $\text{cm}^{-1}$ ) of  $\text{FeSb}_2$  single crystal.

Symmetry	Exp.[14]	$\Omega(0)$	Calculation	Activity	Symmetry	Exp.[11,	Calculation	Activity
						25]		
$A_g^1$	150.7	160.3	146.8	<i>R</i>	$B_{1u}$	195	177.4	<i>IR</i>
$A_g^2$	153.6	164.4	161.2	<i>R</i>	$B_{2u}^1$	106.4	108.1	<i>IR</i>
$B_{1g}^1$	154.3	164.6	173.3	<i>R</i>	$B_{2u}^2$	231.0	210.7	<i>IR</i>
$B_{1g}^2$	173.9	190.4	184.3	<i>R</i>	$B_{2u}^3$	257.0	259.6	<i>IR</i>
$B_{2g}$	90.4		89.4	<i>R</i>		271.0		<i>IR</i>
$B_{3g}$	151.7		95.6	<i>R</i>	$B_{3u}^1$	121.0	122.8	<i>IR</i>
					$B_{3u}^2$	216.0	219.2	<i>IR</i>
					$B_{3u}^3$	261.4	236.6	<i>IR</i>
					$A_u^1$		84.9	<i>Silent</i>
					$A_u^2$		195.2	<i>Silent</i>

$4 \times 4 \times 4$  Monkhorst-Pack  $q$ -points mesh and interpolated along the chosen path. Figure 2(a) shows the calculated phonon dispersions, whereas Fig. 2(b) represents the phonon density of states of  $\text{FeSb}_2$ . It is interesting to note that there is a frequency gap in the phonon dispersion of  $\text{FeSb}_2$  at about  $175 \text{ cm}^{-1}$ . The lower frequency range is dominated by Sb-atoms vibrations (mostly Raman active vibrations), whereas the Fe atoms vibrate at frequencies higher than  $175 \text{ cm}^{-1}$ . These modes are only infrared active.

The phonon density of states peaked structure between 50 and  $90 \text{ cm}^{-1}$  correspond to the low frequency acoustic modes associated with the low-lying  $B_{2g}$  Raman active mode, which calculated frequency is at  $89.4 \text{ cm}^{-1}$ . Sharp peaks in the phonon density of states above  $90 \text{ cm}^{-1}$  come from the flat regions of dispersion curves of corresponding Raman (below  $175 \text{ cm}^{-1}$ ) and infrared (above  $175 \text{ cm}^{-1}$ ) modes.

The lattice dynamics calculations allow us to assign the infrared active modes, experimentally observed in Ref. 11. The assignment of the infrared active modes is done according to the mode energy and symmetry. As we have already mentioned, for  $E||b$  ( $B_{3u}$  symmetry modes) four modes are observed[11] instead of three. We believe that the appearance of two modes at about 257 and  $271 \text{ cm}^{-1}$  instead of a single frequency mode is the consequence of splitting of relatively broad oscillator (which calculated TO frequency is  $259.6 \text{ cm}^{-1}$ ), due to anharmonicity effects.[24] The

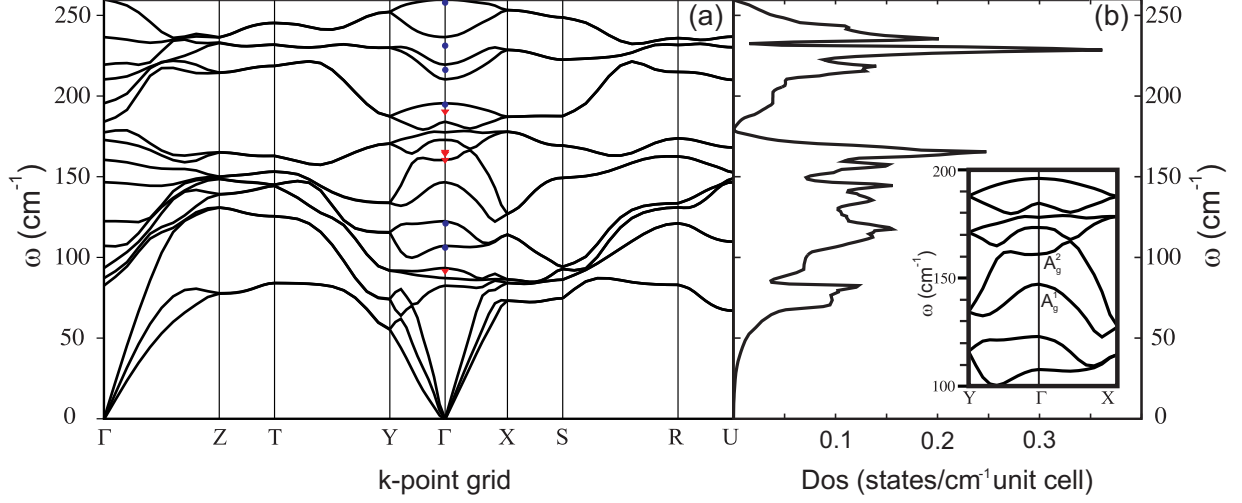


FIG. 2. Phonon dispersion (a) and phonon density of states (b) for FeSb<sub>2</sub>. Triangles and circles represent experimentally observed Raman and infrared mode energies. Inset: Dispersion curves of  $A_g$  phonon modes along the  $\Gamma - Y$  and  $\Gamma - X$  directions.

$B_{1u}$  infrared active mode of FeSb<sub>2</sub> is recently observed at  $195 \text{ cm}^{-1}$  in Ref. 25. The frequencies and assignment of all infrared active modes are given in Table I.

The DFT calculations are performed at zero temperature and should be matched with the phonon energies at zero temperature. For this purpose, we have analyzed the change of the Raman mode energy and linewidth with temperature, induced by anharmonicity effect.

The influence of the anharmonic effects on the Raman mode energy can be taken into account via three- and four-phonon processes by applying the Klemens's ansatz:[26, 27]

$$\begin{aligned}
 \Omega(T) &= \Omega_0 - \Delta^{(3)}(T) - \Delta^{(4)}(T), \\
 \Delta^{(3)}(T) &= C \left( 1 + \frac{2}{e^x - 1} \right), \\
 \Delta^{(4)}(T) &= D \left( 1 + \frac{3}{e^y - 1} + \frac{3}{(e^y - 1)^2} \right),
 \end{aligned} \tag{1}$$

where  $\Omega_0$  is the temperature independent contributions to the Raman mode energy,  $C$  ( $D$ ) is the three (four)-phonon anharmonic constant,  $x = \hbar\Omega_0/2k_B T$  and  $y = \hbar\Omega_0/3k_B T$ .

There are two main contributions to the phonon linewidth: (i) anharmonic decay of the phonon, and (ii) perturbation of the translational symmetry of the crystal by the presence of impurities

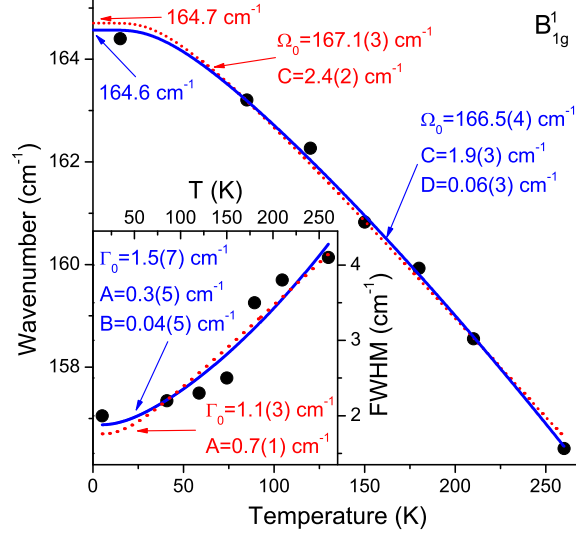


FIG. 3. (Color online)  $B_{1g}^1$  mode wavenumber as a function of temperature. Solid line represents theoretical extrapolation by using Eq. (1), whereas dashed line represent theoretical extrapolation obtained by omitting four-phonon contribution in Eq. (1). Inset: Theoretical calculation of FWHM obtained by using Eq. (2) (solid line) and by omitting four-phonon contribution in Eq. (2) (dashed line).

and defects. Having this in mind, the phonon linewidth can be described with:

$$\begin{aligned}\Gamma(T) &= \Gamma_0 + \Gamma^{(3)}(T) + \Gamma^{(4)}(T), \\ \Gamma^{(3)}(T) &= A \left( 1 + \frac{2}{e^x - 1} \right) \\ \Gamma^{(4)}(T) &= B \left( 1 + \frac{3}{e^y - 1} + \frac{3}{(e^y - 1)^2} \right)\end{aligned}\quad (2)$$

where  $\Gamma_0$  is the temperature independent linewidth, which originates mainly from (ii),  $A$  ( $B$ ) is the three (four)-phonon anharmonic constant. Analysis of energy and FWHM (full width at half maximum) vs. temperature for the  $B_{1g}^1$  mode is presented in Fig. 3. Because anharmonicity constants ratio  $B/A$  and  $D/C$  is very small, see Fig. 3, the contribution of the four-phonon processes is small compared to that of the three-phonon processes. The obtained value of  $\Omega(0) = 164.6 \text{ cm}^{-1}$  for this mode at zero temperature is in good agreement with the DFT results. Similar analysis have been performed for  $B_{2g}^2$  symmetry mode giving the value of  $\Omega(0) = 190.4 \text{ cm}^{-1}$  at zero temperature,[15] which is in rather good agreement with our calculations.

The calculated energy ( $89.4 \text{ cm}^{-1}$ ) for the  $B_{2g}$  symmetry mode in the  $\Gamma$  point shows excellent agreement with the room temperature experimental data. This is to be expected since low energy modes show week anharmonicity effects. Surprisingly large discrepancy between experimental and calculated phonon energies is observed for the  $B_{3g}$  mode. Since the  $B_{2g}$  and  $B_{3g}$  modes have similar

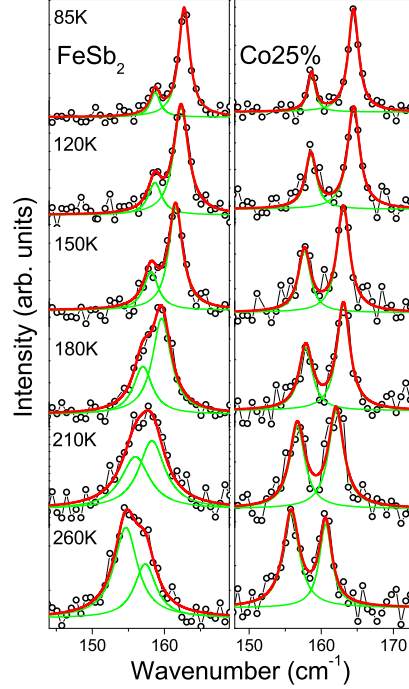


FIG. 4. (Color online) The Raman scattering spectra of  $\text{FeSb}_2$  (left panel)[15] and  $\text{Fe}_{0.75}\text{Co}_{0.25}\text{Sb}_2$  (right panel) single crystals in the  $(x'x')$ ,  $x' = \frac{1}{\sqrt{2}}[101]$ , configuration ( $A_g$  symmetry modes) measured at various temperatures.

normal modes, the chain rotation around the  $x$  and  $y$  axis, respectively (see Fig. 1) their frequencies should be very close. This large disagreement is also unexpected since all other calculated phonon energies show rather good agreement with the experimentally obtained data. By detailed inspection of our previously published Raman spectra[14] of pure, Co and Cr doped  $\text{FeSb}_2$  samples we did not find any mode in a low frequency region close to the calculated frequency ( $95 \text{ cm}^{-1}$ ) for the  $B_{3g}$  mode. The missing  $B_{3g}$  mode is most probably of a very low intensity and it was not possible to extract it from the noise. The mode observed at  $151.7 \text{ cm}^{-1}$  for  $(x'y)$  polarization, which we assigned in Ref. 14 as the  $B_{3g}$  mode, could be the "leakage" of the  $A_g^1$  mode, which appears at about  $150.7 \text{ cm}^{-1}$  in the  $(x'x')$  polarization.

It is interesting to note that the dispersion curves of two  $A_g$  symmetry Raman modes have opposite slopes near the  $\Gamma$  point (see the inset of Fig. 2(b)), which leads to the mode mixing with the "anticrossing" effect.  $A_g^1$  mode represents stretching vibration of Sb ions, whereas  $A_g^2$  mode represents twisting of Sb ions which tend to rotate Sb ions around the  $z$ -axis, see Fig 1. In our previous paper,[15] we showed the existence of the  $A_g$  mode mixing in the case of pure  $\text{FeSb}_2$  and Cr alloyed samples. Here we present detailed analysis of the mixing of two  $A_g$  modes for pure and 25% Co alloyed samples.



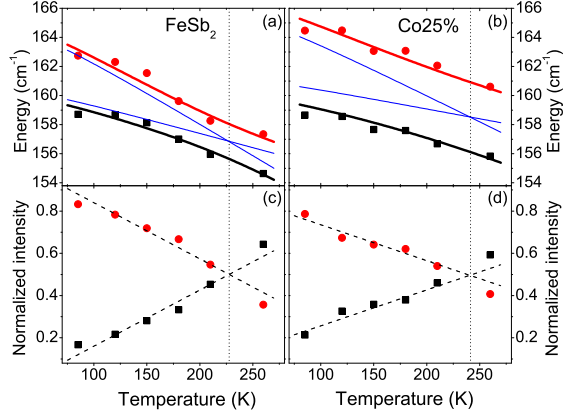


FIG. 5. (Color online) Energies (a), (b) and normalized intensities (c), (d) as a function of temperature of the  $A_g$  modes for  $\text{FeSb}_2$  and  $\text{Fe}_{0.75}\text{Co}_{0.25}\text{Sb}_2$  single crystals. Thin solid lines show energy vs temperature dependence of the  $A_g$  modes without coupling. Thick solid lines (red and black) show mode energy temperature dependence for two coupled  $A_g$  modes calculated using Eq. (4). The dashed lines are guide to the eye.

The polarized Raman scattering spectra for pure  $\text{FeSb}_2$  (left panel[15]) and  $\text{Fe}_{0.75}\text{Co}_{0.25}\text{Sb}_2$  (right panel) single crystals, measured in the  $(x'x')$  configuration ( $A_g$  modes) at different temperatures, are presented in Fig. 4. The Lorentzian lineshape profile has been used for the extraction of mode energy and linewidth. Fig. 5 shows the energies and normalized intensities as a function of temperature of the  $A_g$  modes for  $\text{FeSb}_2$  and  $\text{Fe}_{0.75}\text{Co}_{0.25}\text{Sb}_2$  single crystals. In the observed temperature range, energies of two  $A_g$  modes for pure and 25% Co doped samples are very close which implies the existence of the mode mixing, manifested by mode repulsion and intensity transfer with the change of temperature.[28] Indeed, intensities of these modes are exchanged for both samples in the temperature range between 210 and 260 K (see Figs. 4 and 5).

In general, two phonon branches or any other elementary excitations of the same symmetry, may couple leading to the renormalization of the quasiparticle energies. Coupling between two phonon branches yields to the energy and linewidth changes (anticrossing effect). We can consider the coupling of two phonon branches as coupling of two quantum oscillators. When the perturbation is small, we can write the Hamiltonian of the system as

$$\hat{H} = \begin{bmatrix} \Omega_1(T) & V \\ V & \Omega_2(T) \end{bmatrix}, \quad (3)$$

where  $V$  is the interaction constant,  $\Omega_1(T)$  and  $\Omega_2(T)$  are the unperturbed mode energies, obtained by taking into account, due to simplicity, only three-phonon process in Eq. (1). The eigenvalues

TABLE II. Best fit parameters for energy temperature dependence of the  $A_g$  symmetry modes using Eq. (4).

Compound	Symmetry	$\Omega_0$ (cm $^{-1}$ )	$C$ (cm $^{-1}$ )	$V$ (cm $^{-1}$ )
FeSb $_2$	$A_g^1$	167.1	2.65	1.2
	$A_g^2$	161.5	1.16	
Fe $_{0.75}$ Co $_{0.25}$ Sb $_2$	$A_g^1$	167.5	2.2	2.4
	$A_g^2$	161.9	0.80	

of the Hamiltonian are given by

$$\omega_{\pm} = \frac{1}{2} \left( \Omega_1(T) + \Omega_2(T) \pm \sqrt{(\Omega_1(T) - \Omega_2(T))^2 + 4V^2} \right). \quad (4)$$

Eq. (4) gives a rather good fit of the experimental data (solid lines in Fig. 5 (a),(b)), suggesting the absence of any additional temperature dependent couplings (i.e. electron-phonon interaction) for these modes. Fitting parameters are presented in Table II. Zero-temperature energies of  $A_g^1$  and  $A_g^2$  symmetry modes, in the absence of interaction, for pure (25% Co doped) sample are  $\Omega_1(0) = 160.3$  cm $^{-1}$  and  $\Omega_2(0) = 164.5$  cm $^{-1}$  ( $\Omega_1(0) = 161.1$  cm $^{-1}$  and  $\Omega_2(0) = 165.3$  cm $^{-1}$ ). One can notice that the zero-temperature energies for decoupled modes are increased by 0.8 cm $^{-1}$  (about 0.5% increase) with 25% Co doping, corresponding to the unit cell volume contraction.[3] The phonon energy of the bond-stretching mode scales as  $R^{-3}$ , where  $R$  is the bond length.[29] Since the change in  $R^{-3}$  is proportional to the inverse volume change, we can expect the phonon-energy change for bond-stretching modes ( $A_g$  modes) to be inversely proportional to the volume change. Because the Co atom substitutes Fe atom, which is located in the center of the inversion, there is no change in Raman spectra due to the mass effect. Additional repulsion between the coupled modes are due to the interaction. With Co doping, the interaction constant  $V$  increases, resulting in larger mode separation for the 25% doped sample.

## V. CONCLUSION

In summary, we presented a detailed theoretical and experimental study of the FeSb $_2$  phonon dynamics. All experimentally observed Raman and infra-red active modes were successfully assigned. The calculated phonon frequencies in the  $\Gamma$  point agree with the measured frequencies. We believe that the low energy  $B_{3g}$  mode is of a very low intensity and therefore is not observed in the Raman experiments. The phonon mode at 150.7 cm $^{-1}$ , which we previously assigned as the  $B_{3g}$

mode, could be the "leakage" of the  $A_g^1$  mode. The strong intensity exchange of the  $A_g$  symmetry modes, observed in our Raman scattering experiments in the temperature range between 210 K and 260 K, is successfully described by a simple model of coupling of two phonon branches with the same symmetry. The mode mixing is also implied from the calculated dispersion curves, which show opposite slopes for two  $A_g$  modes near the  $\Gamma$  point. We find that doping of FeSb<sub>2</sub> with Co increases the  $A_g$  modes repulsion.

### ACKNOWLEDGMENT

This work was supported by the Serbian Ministry of Education and Science under Projects ON171032, III45018, ON171017. Part of this work (C. P. and R. H.) was carried out at the Brookhaven National Laboratory which is operated for the Office of Basic Energy Sciences, U.S. Department of Energy by Brookhaven Science Associates (DE-Ac02-98CH10886). Numerical simulations were run on the AEGIS e-Infrastructure, supported in part by FP7 projects EGI-InSPIRE, PRACE-1IP and HP-SEE. Z.V.P. and M.M.R. acknowledge support from the Swiss National Science Foundation through the SCOPES Grant No. IZ73Z0-128169.

\* Present address: Department of Physics, University of Maryland, College Park MD 20742-4111, USA.

- 
- [1] C. Petrovic, J. W. Kim, S. L. Bud'ko, A. I. Goldman P. C. Canfield, W. Choe, and G. J. Miller, *Phys. Rev. B* **67**, 155205 (2003).
  - [2] C. Petrovic, Y. Lee, T. Vogt, N. D. Lazarov, S. L. Bud'ko, and P. C. Canfield, *Phys. Rev. B* **72**, 045103 (2005).
  - [3] Rongwei Hu, V. F. Mitrović, and C. Petrovic, *Phys. Rev. B* **74**, 195130 (2006).
  - [4] Rongwei Hu, V. F. Mitrović, and C. Petrovic, *Phys. Rev. B* **76**, 115105 (2007).
  - [5] A. Bentien, S. Johnsen, G. K. H. Madsen, B. B. Iversen, and F. Steglich, *Europhys. Lett.* **80**, 39901 (2007).
  - [6] Rongwei Hu, V. F. Mitrović, and C. Petrovic, *Appl. Phys. Lett.* **92**, 182108 (2008).
  - [7] P. Sun, N. Oeschler, S. Johnsen, B. B. Iversen, and F. Steglich, *Dalton Trans.* **39**, 1012 (2010).
  - [8] Peijie Sun, Niels Oeschler, Simon Johnsen, Bo Brummerstedt Iversen, and Frank Steglich, *Phys. Rev. B* **79**, 153308 (2009).
  - [9] H. Takahashi, Y. Yasui, I. Terasaki and M. Sato, *J. Phys. Soc. Japan* **80**, 154708 (2011).
  - [10] J. M. Tomczak, K. Haule, T. Miyake, A. Georges, and G. Kotliar, *Phys. Rev. B* **82**, 085104 (2010).
  - [11] A. Perucchi, L. Degiorgi, Rongwei Hu, C. Petrovic, and V.F. Mitrović, *Eur. Phys. J. B* **54**, 175 (2006).

- [12] H. D. Lutz and B. Müller, *Phys. Chem. Miner.* **18**, 265 (1991).
- [13] A. M. Racu, D. Menzel, J. Schoenes, M. Marutzky, S. Johnsen, and B. B. Iversen, *J. Appl. Phys.* **103**, 07C912 (2008).
- [14] N. Lazarević, Z. V. Popović, Rongwei Hu, and C. Petrovic, *Phys. Rev. B* **80**, 014302 (2009).
- [15] N. Lazarević, Z. V. Popović, Rongwei Hu, and C. Petrovic, *Phys. Rev. B* **81**, 144302 (2010).
- [16] H. Holseth, and A. Kjekshus, *Acta Chem. Scand.* **22**, 3273 (1968).
- [17] H. Holseth, A. Kjekshus, and A. F. Andresen, *Acta Chem. Scand.* **24**, 3309 (1970).
- [18] <http://www.quantum-espresso.org/pseudo.php>.
- [19] P. Giannozzi, S. Baroni, N. Bonini, M. Calandra, R. Car, C. Cavazzoni, D. Ceresoli, G. L Chiarotti, M. Cococcioni, I. Dabo, A. Dal Corso, S. de Gironcoli, S. Fabris, G. Fratesi, R. Gebauer, U. Gerstmann, C. Gougoussis, A. Kokalj, M. Lazzeri, L. Martin-Samos, N. Marzari, F. Mauri, R. Mazzarello, S. Paolini, A. Pasquarello, L. Paulatto, C. Sbraccia, S. Scandolo, G. Sclauzero, A. P Seitsonen, A. Smogunov, P. Umari, and R. M Wentzcovitch, *J. Phys. Condens. Matter* **21**, 395502 (2009).
- [20] N. Marzari, D. Vanderbilt, A. De Vita, and M. C. Payne, *Phys. Rev. Lett.* **82**, 3296 (1999).
- [21] A. V. Lukoyanov, V. V. Mazurenko, V. I. Anisimov, M. Sigrist, and T. M. Rice, *Eur. Phys. J. B* **53**, 205 (2006).
- [22] A. Bentien, G. K. H. Madson, S. Johnsen, and B. B. Iversen, *Phys. Rev. B* **74**, 205105 (2006).
- [23] S. Baroni, S. de Gironcoli, A. Dal Corso, and P. Giannozzi, *Rev. Mod. Phys.* **73**, 515 (2001).
- [24] F. Gervais and B. Piriou, *Phys. Rev. B* **10**, 1642 (1974).
- [25] A. Herzog, M. Marutzky, J. Sichelschmidt, F. Steglich, S. Kimura, S. Johnsen, and B. B. Iversen, *Phys. Rev. B* **82**, 245205 (2010).
- [26] M. Balkanski, R. F. Wallis, and E. Haro, *Phys. Rev. B* **28**, 1928 (1983).
- [27] P. G. Klemens, *Phys. Rev.* **148**, 845 (1966).
- [28] M. N. Iliev, M. V. Abrashev, J. Laverdier, S. Jandl, M. M. Gospodinov, Y.-Q. Wang, and Y.-Y. Sun, *Phys. Rev. B* **73**, 064302 (2006).
- [29] Z. V. Popović, V Stergiou, Y. S. Raptis, M. J. Konstantinović, M. Isobe, Y. Ueda, and V. V. Moshchalkov, *J. Phys.: Condens. Matter* **14**, L583 (2002).